

Cascade Appearance Signatures of Sterile Neutrinos at 1-100 TeV

B. R. Smithers,^{1,*} B. J. P. Jones,¹ C. A. Argüelles,² J. M. Conrad,³ and A. Diaz³

¹*Department of Physics, University of Texas at Arlington, Arlington, Texas 76019, USA*

²*Department of Physics, Harvard University, Cambridge, Massachusetts, USA*

³*Dept. of Physics, Massachusetts Institute of Technology, Cambridge, MA 02139, USA*

(Dated: February 15, 2022)

Neutrino telescopes provide strong sensitivity to sterile neutrino oscillations through matter-effects occurring in the few TeV energy range for eV²-scale neutrino mass-squared splittings. Prior searches have focused on ν_μ disappearance, which has a particularly strong sensitivity to the mixing angle θ_{24} via $\nu_\mu \rightarrow \nu_s$ transitions. Nowadays, the $\nu_\mu \rightarrow \nu_e$ and $\nu_\mu \rightarrow \nu_\tau$ appearance channels have been considered less promising at neutrino telescopes, due in part to the much smaller target volume for cascades relative to tracks. This work explores the detectability of these signatures at neutrino telescopes given present constraints on sterile neutrino mixing, and as an example, forecasts the sensitivity of the IceCube Neutrino Observatory to the mixing angles θ_{14} , θ_{24} , and θ_{34} in the 3+1 sterile neutrino model using the cascade channel with ten years of data. We find that ν_τ appearance signatures consistent with the existing IceCube ν_μ disappearance best-fit point are discoverable for values of θ_{34} consistent with world constraints, and that the sterile neutrino parameters favored by the BEST and gallium anomalies are expected to be testable at the 95% confidence level.

I. INTRODUCTION

The three-mass and three active-flavor neutrino paradigm has been well-studied [39, 40, 55, 76, 77, 79]. However, several anomalies persist at short baselines, including in $\nu_\mu \rightarrow \nu_e$ appearance in decay-in-flight [27] and decay-at-rest [34] beams and $\nu_e \rightarrow \nu_e$ disappearance at reactors [70, 78] and with ⁷¹Ga electron capture sources [20, 60]. These anomalies have been attributed to possible oscillations of unknown neutrinos with mass-squared differences in the range of $\Delta m^2 \sim 0.1 - 10 \text{ eV}^2$ [15]. Such an additional neutrino flavor state must be non-weakly interacting, or “sterile,” to be consistent with observed decay widths of the Z-boson [77]; the simplest such model is known as the “3+1” light sterile neutrino model in which a single sterile neutrino is added.

There have been interesting recent developments for the 3+1 model. The BEST experiment appears to validate the anomalous electron neutrino disappearance signature of the previous gallium anomalies with a new level of statistical significance and experimental precision [37]. The Neutrino-4 experiment claims evidence of short-baseline oscillations in the $\bar{\nu}_e$ disappearance channel with $\Delta m^2 \sim 7.3 \text{ eV}^2$ at the 2.9σ level. Meanwhile results from the MicroBooNE [22–24] experiment challenge the interpretation that the MiniBooNE low energy excess [26] is due entirely to the electron neutrino by placing a constraint on the sterile neutrino interpretation of the excess; though the impact of this observation on the 3+1 model is just beginning to be assessed [33, 48]. Continued exploration of sterile neutrino mixing in all channels and all energy ranges thus remains strongly motivated [69].

The addition of a fourth neutrino mass and flavor eigenstate expands the unitary mixing matrix to four dimensions. The four-neutrino oscillations model becomes an extension of the three-neutrino model with three additional mixing angles θ_{14} , θ_{24} , and θ_{34} , and two new CP-violating phases δ_{14} and δ_{24} . These three new mixing angles parametrize the amplitude of oscillations between the three active states and the one sterile state, and lead to additional short-baseline vacuum-like oscillations as well as novel effects in the presence of matter [28, 29, 42, 43, 67]. In this work we consider CP-conserving models with all CP-violating phases set to zero.

Of particular interest to neutrino telescopes, matter effects can result in the near complete disappearance of TeV-scale muon anti-neutrinos passing through the Earth’s core for a sterile neutrino with eV-scale mass squared differences [36, 44, 51, 53, 68, 72, 74]. This signature of matter-enhanced resonant disappearance has been targeted by the IceCube Neutrino Observatory [12, 13], leading to one of the most sensitive ν_μ disappearance analyses to date. The result of the analysis was a closed 90% contour with best fit point at $\sin^2 2\theta_{24} \sim 0.1$ and $\Delta m_{41}^2 = 4.5 \text{ eV}^2$, under a conservative assumption (for the ν_μ disappearance channel) that $\theta_{34} = \theta_{14} = 0$. In addition to being a strong refutation, lower mass solutions consistent with the LSND [34] and MiniBooNE anomalies and constraints around 1 eV^2 [15, 45, 47, 49, 59, 66], a possible interpretation of this result is as a statistically weak hint of a disappearance signature around $\Delta m_{41}^2 \sim 4.5 \text{ eV}^2$. Further exploration of this region of parameter space in other channels at neutrino telescopes is therefore strongly motivated.

In this work, we explore the potential of sterile neutrino searches at gigaton-scale neutrino telescopes using matter-enhanced ν_τ and ν_e appearance signatures that occur when either θ_{34} or θ_{14} are non-zero [52]. We will show that ν_τ appearance of considerable strength may

* Corresponding author: benjamin.smithers@mavs.uta.edu

accompany ν_μ disappearance within the IceCube allowed region for Δm_{41}^2 and θ_{24} , for values of θ_{34} that remain consistent with world data sets. We will also demonstrate that these signatures can be probed using IceCube’s public data samples. Finally, we will also explore possible sensitivity to ν_e appearance at levels consistent with the gallium and BEST anomalies.

The IceCube Neutrino Observatory is described at length in Ref. [1]. Briefly, the detector is a cubic-kilometer Cherenkov neutrino observatory one and half kilometers deep in the Antarctic ice [1]. There, 5160 photo-multiplier tubes encased within glass pressure vessels, or “Digital Optical Modules” (DOMs) [16] detect Cherenkov emission from charged particles traversing the ice. The DOMs are arranged vertically with a seventeen meter spacing into seventy-nine strings, which themselves are aligned into a hexagonal lattice with a 125 meter spacing. An additional, more densely instrumented sub-detector called DeepCore exists towards the bottom-center of the main detector [17]. The observatory has been running for over a decade and has accumulated large numbers of ν_μ CC interactions which make depositions of light that make long signatures in the detector called tracks; and neutral current, electron neutrino, and tau neutrino events which deposit light in blob-like shapes called cascades. These event topologies are elaborated upon in Section II.

IceCube analyses targeting ν_μ disappearance are considered track-like only, since the only available signature under the previous mixing assumptions $\theta_{14} = \theta_{34} = 0$ is $\nu_\mu \rightarrow \nu_s$ disappearance. In similar models with both non-zero θ_{24} and θ_{34} , however, resonant $\nu_\mu \rightarrow \nu_\tau$ oscillations lead to a strong appearance signature of ν_τ as shown in Figure 1. While some of the ν_τ will produce τ^\pm that decay leptonically to produce additional tracks, dampening the ν_μ disappearance signature, most charged current ν_τ and $\bar{\nu}_\tau$ interactions will produce localized energy deposits that will be reconstructed as single cascades at these energies [18]. As in the $\nu_\mu \rightarrow \nu_s$ channel, the most striking feature of the signature is a resonant flavor oscillation for Earth-core-crossing anti-neutrinos at a specific energy, proportional to the sterile neutrino Δm_{41}^2 value. Since this matter effect occurs because of an interference between the vacuum oscillation phase and the matter-driven phase, the latter changing sign between neutrinos and anti-neutrinos, for small mixing angles the resonance is only present in for anti-neutrinos, given a heavier sterile neutrino. The appearance probabilities for $\nu_\mu \rightarrow \nu_\tau$ and $\bar{\nu}_\mu \rightarrow \bar{\nu}_\tau$ are shown separately in Figure 2.

For zero θ_{24} very little signal is expected since the muon neutrinos, which dominate the flux at IceCube, cease to mix with the heavier mass state. As a consequence there will be negligible ν_τ appearance, regardless of the value of θ_{34} . However, recent IceCube results favor a non-zero value for $\sin^2(2\theta_{24})$ of around 0.1, and assuming ν_μ/ν_4 mixing at this level, the observable ν_τ appearance will depend strongly on the value of θ_{34} . At the smallest values of θ_{34} ($\theta_{34} \lesssim 0.1$), $\nu_\mu \rightarrow \nu_s$ oscil-

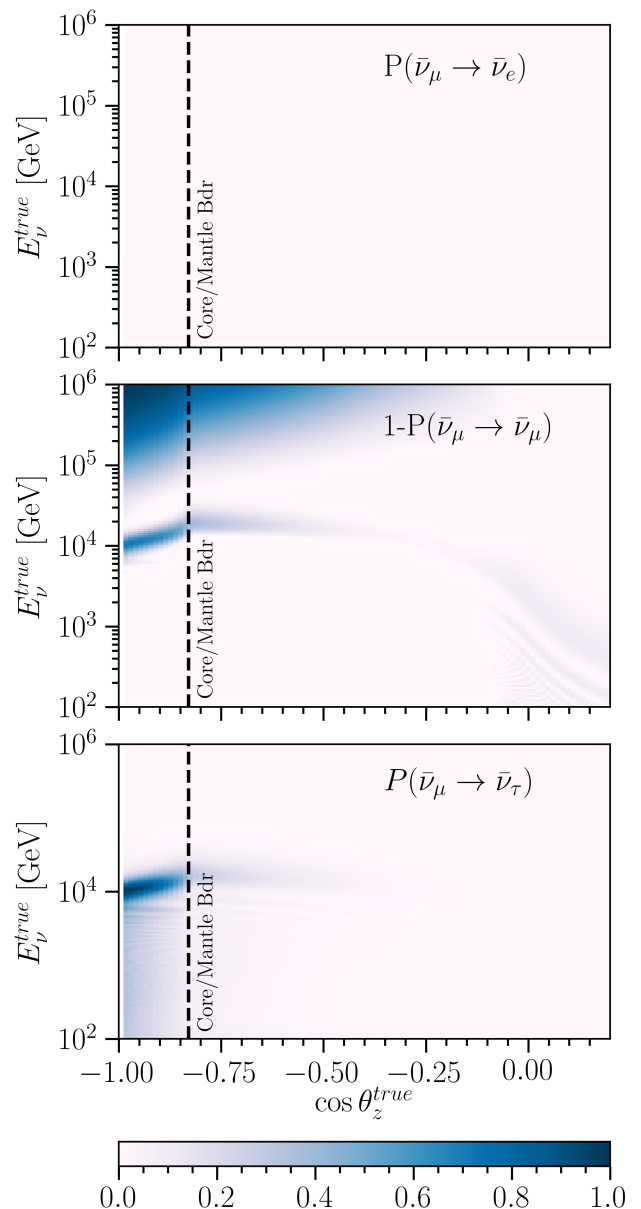


FIG. 1. Transition probabilities $P(\bar{\nu}_\mu \rightarrow \bar{\nu}_\alpha)$ for $\bar{\nu}_e$ (top), $\bar{\nu}_\mu$ (middle), and $\bar{\nu}_\tau$ (bottom) for a sterile neutrino flux with $\sin^2(2\theta_{24}) = 0.1$, $\sin^2(2\theta_{34}) = 0.2$, and $\Delta m_{41}^2 = 4.5 \text{ eV}^2$. A dashed black line is used to denote the outer core-mantle boundary, and a solid black line denotes the inner-outer core boundary. These probabilities are shown as a function of the neutrino’s energy (E_ν^{true}) and the cosine of the angle measured from an upwards direction, towards the neutrino’s origin.

lations dominate over $\nu_\mu \rightarrow \nu_\tau$ appearance from standard oscillations, and ν_μ disappearance is the only visible signature. For values of θ_{34} larger than this threshold, the $\nu_\mu \rightarrow \nu_\tau$ oscillations begin to dominate and ν_τ appearance manifests, leading to the appearance signature shown in Figure 1 (bottom). Increasing Δm_{41}^2 has

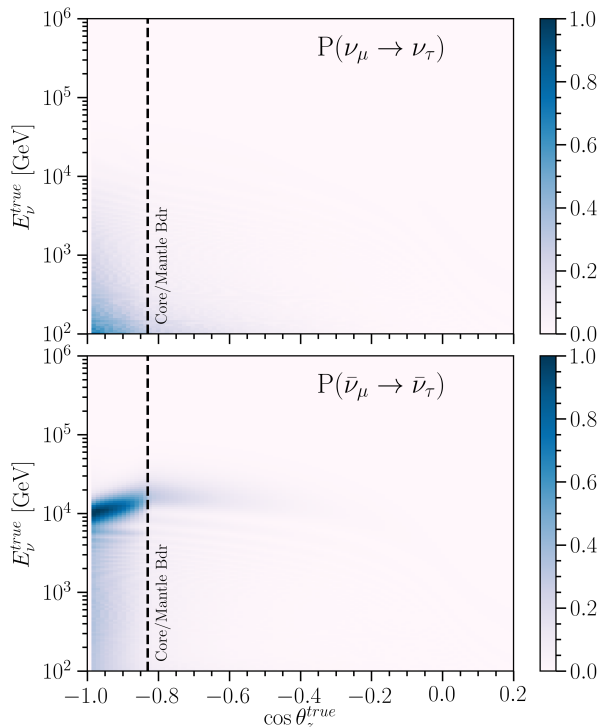


FIG. 2. Appearance probabilities for $P(\nu_\mu \rightarrow \nu_\tau)$ (top) and $P(\bar{\nu}_\mu \rightarrow \bar{\nu}_\tau)$ (bottom) for a sterile neutrino flux with $\sin^2(2\theta_{24}) = 0.1$, $\sin^2(2\theta_{34}) = 0.19$, and $\Delta m_{41}^2 = 4.5 \text{ eV}^2$.

the effect of broadening the appearance signature until $\sim 10 \text{ eV}^2$, after which raising the mass-squared splitting has only a marginal effect. Increasing θ_{24} while reducing θ_{34} proportionately leaves the appearance signatures mostly unchanged while diminishing the disappearance amplitude.

In addition, the effects of non-zero mixing angle θ_{14} can also be considered, having the consequence of introducing similar appearance signatures into the ν_e appearance channel [80]. For practical purposes ν_e and ν_τ charged current events are indistinguishable at these energies in IceCube. Notably, neutrino telescopes are the only experiments in the world with substantial sensitivity to sterile-neutrino induced ν_τ appearance, so such direct constraints on the θ_{34} parameter are specific to these programs. Constraints on θ_{14} , on the other hand, may directly relate to anomalies in $\nu_\mu \rightarrow \nu_e$ and ν_e disappearance. As we will show, constraining the ν_e appearance signature at IceCube under the non-zero presently favored value of θ_{24} from ν_μ disappearance have direct implications for the BEST anomaly and the associated reactor- $\bar{\nu}$ anomaly.

This rich phenomenology motivates multi-mixing-angle and multi-channel searches to fully explore sterile neutrino mixing around the matter resonance at neutrino telescopes. In this work, we explore this space of mixing parameters by using publicly available tools, effective areas, and Monte Carlo simulation to estimate IceCube's

sensitivity to θ_{24} , θ_{34} , and Δm_{41}^2 through cascades.

II. NEUTRINO ENERGY DEPOSITION

Large-volume neutrino telescopes typically are sensitive in the TeV to PeV energies; here, Deep-Inelastic Scattering (DIS) [58] and the recently-observed [14] Glashow-Resonance [61] interactions dominate. The detected neutrino interaction events fall into two morphological categories: tracks and cascades.

Charged-current (CC) ν_μ DIS events result in muons at energies where radiative processes dominate energy loss rates. As a result, energy losses are stochastically driven and the produced muons travel for kilometers. The results are threefold: muons are difficult to fully contain in neutrino telescopes, muon energies are poorly correlated with progenitor muon-neutrino energies, and muons' long travel-distance can allow for reconstructing their direction to within 1° [7]. These events are called *tracks* [3].

All neutral-current (NC) DIS events result in a hadronic shower spreading around the interaction point and a secondary neutrino invisibly carrying away a proportion of the parent neutrino's energy. These events are often contained with a spherical topology. ν_e -CC interactions develop similarly to neutral-current interactions, but repeated inverse Compton scattering of the produced electron initiates an electromagnetic shower superimposed over the hadronic shower. Thus, nearly all of the interacting neutrino's energy is observable as detectable light. These events are called *cascades*. Such events tend to be well-contained permitting an efficient energy reconstruction, although suffer from poor angular reconstruction [3].

The evolution of a ν_τ -CC interaction is highly dependent on the energies involved. A tau is produced simultaneously as a hadronic cascade propagates around the interaction point, and then the tau decays. Due to their large mass, taus have a short lifetime and a decay length of $\sim 50 \text{ m}$ per PeV of tau energy [18]. From the tau branching ratios [79], 17.37% of the charged tau decays evolve as muon tracks, while the remainder of the decays evolve as electromagnetic or hadronic cascades. Only at neutrino energies above 60 TeV do ν_τ -CC interactions yield events with distinguishable primary and secondary cascades [18].

Several distinct event samples have been developed to study these different types of events in IceCube. The High-Energy Starting Events sample [19], for example, was developed to study both taus and high-energy neutrinos likely astrophysical in origin. There exist other events samples optimized for higher event rates at lower energies, such as the Medium-Energy Starting Events [4], and the five-year inelasticity sample [10]. There are also samples optimized for muon purity, such as the eight-year atmospheric muon sample [13] and others optimized for accurate energy resolution such as the six-years cascade sample [11]. This work will consider the cascade event

selection described in [71] and the track event selection previously used in IceCube sterile neutrino searches [6].

III. NEUTRINO FLUXES

We calculate the expected event rates in IceCube exclusively using publicly available data on effective areas and publicly available Monte Carlo simulation samples. By studying the expected event rates in both track and cascade channels, we are able to estimate IceCube's sensitivities to sterile neutrino parameters given the existing ten year data set. At sensitive energies there are two relevant neutrino populations whose flux must be modeled: atmospheric and astrophysical neutrinos.

Predicting atmospheric neutrino event rates requires a progenitor cosmic-ray flux, simulation of resulting air showers, propagation of the shower-born neutrinos through the Earth, and convolution of these fluxes with effective areas for a given sample selection to yield a final predicted event rate. For this work, we use the MCEq cascade equation solver [56] with the three-population Hillas-Gaisser 2012 H3a cosmic-ray flux model [57] and using the SYBILL 2.3c hadronic interaction model [75] to simulate air showers. The Poly-Gonato model for the cosmic-ray flux [64] and QGSJET-II-04 model for hadronic interactions [73] were also found to produce similar results for this analysis.

These fluxes are then propagated through the Earth using the Simple Quantum Integro-Differential Solver for neutrino oscillations (nuSQuIDS) [31, 32, 41]. We have configured nuSQuIDS to propagate the fluxes according to a spherically-symmetric Preliminary Reference Earth Model (PREM) [50]; where it accounts for both coherent and non-coherent interactions relevant at these energies [61, 62] as well as tau-neutrino regeneration [63]. For this work we use the CSMS cross sections [46]. We fix the three-neutrino oscillations parameters to their global best-fit values [54].

Astrophysical neutrino event rates are calculated similarly. Although, the neutrino flux prior to propagation through the Earth instead is expected to follow a power-law spectrum as a function of neutrino energy E_ν ,

$$\Phi_{astr,\alpha}(E_\nu) = r_\alpha \Phi_0 \left(\frac{E_\nu}{E_0} \right)^{-\gamma}, \quad (1)$$

normalized at $E_0 = 100$ TeV and with $\Phi_0 = 2.85 \times 10^{-18} [\text{GeV} \cdot \text{cm}^2 \cdot \text{sr} \cdot \text{s}]^{-1}$, a spectral index of $\gamma = 2.39$ [13], and a flavor-ratio r_α for $\alpha \in (e, \mu, \tau)$. The flux is assumed isotropic and to have a $\nu : \bar{\nu}$ ratio of 1 : 1. Astrophysical neutrinos are assumed to be created with regards to the pion-decay induced flavor ratio of 1:2:0 [35, 38]; these are then propagated through vacuum over large energy-baseline ratios, recovering the expected $\frac{1}{3} : \frac{1}{3} : \frac{1}{3}$ flavor ratio at Earth for the three-neutrino model [5]. The same is done for sterile-neutrino hypotheses to predict expected four-flavor flavor ratios [30].

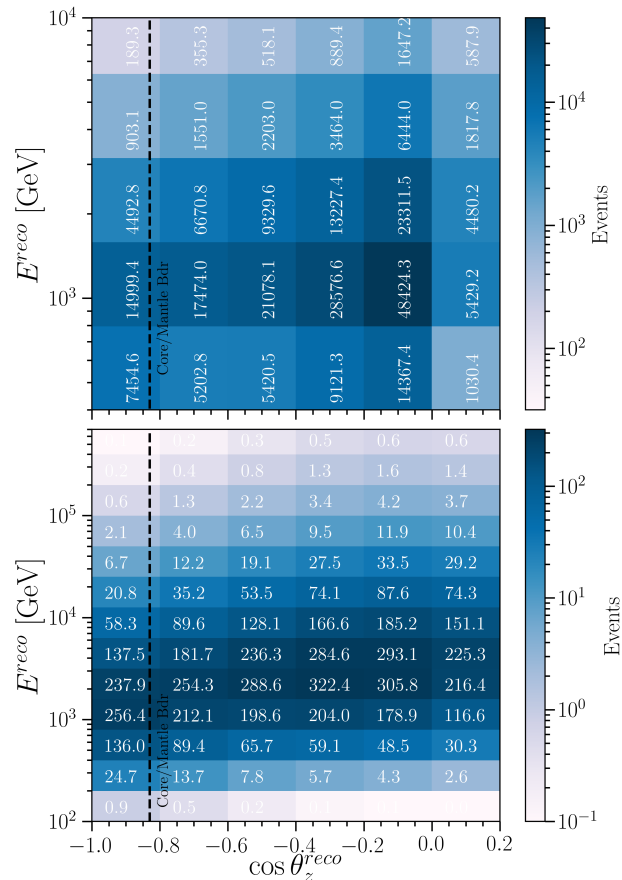


FIG. 3. Expected number of through-going tracks (top) and cascades (bottom) for ten years of livetime using the Hillas Gaisser H3a cosmic ray flux model, SYBILL 2.3c interaction model, and the event selection described in Ref [71].

A. Cascade Rates

Total cascade event rates in IceCube are calculated bin-wise, linearly in $\log(E^{\text{true}})$ and $\cos \theta_z^{\text{true}}$, by integrating over a product of flux and effective area A_{eff} in each bin (i,j), summing for each neutrino species α , and multiplying by livetime τ . This is shown below in Equation 2.

$$N_{i,j}^{evt} = 2\pi\tau \sum_{\alpha} \int_{E_i}^{E_{i+1}} dE_{\nu}^{\text{true}} \int_{\cos \theta_j}^{\cos \theta_{j+1}} d(\cos \theta_z^{\text{true}}) \times \Phi_{\alpha}(E_{\nu}^{\text{true}}, \cos \theta_z) A_{eff,\alpha}(E_{\nu}^{\text{true}}, \cos \theta_z^{\text{true}}) \quad (2)$$

The effective areas used are publicly available and determined from the gradient boosted decision tree methods event selection developed and available in Ref. [71]. Expected bin-wise event counts N_{mn}^{mn} at reconstructed energy $(E_{\nu}^{\text{reco}})_m$ and zenith $(\cos \theta_z^{\text{reco}})_n$ follow from smearing from these expected true values by a bin-to-bin reconstruction probability P_{mn}^{ij} ,

$$N_{mn}^{\text{reco}} = N_{ij}^{\text{true}} P_{ijmn}. \quad (3)$$

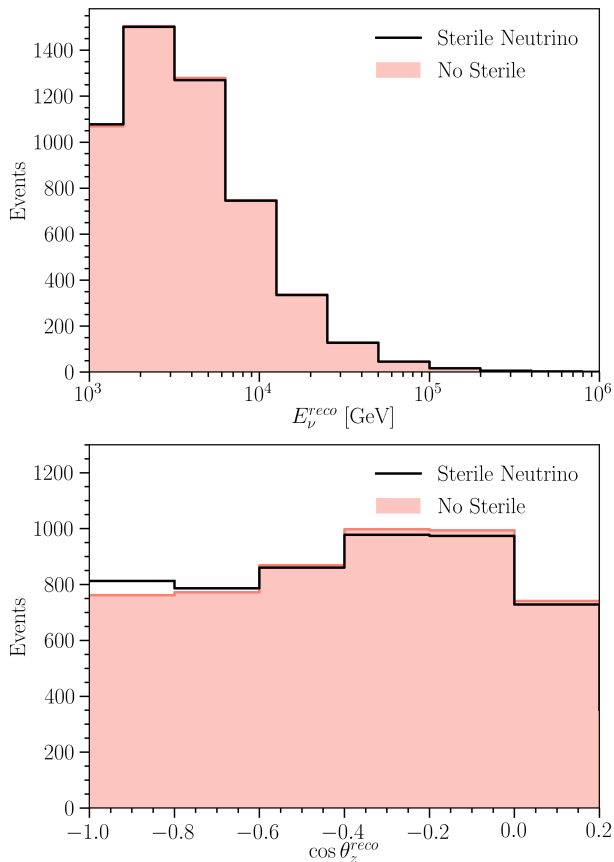


FIG. 4. Expected number of cascades for ten years of livetime using the Hillas Gaisser H3a cosmic-ray flux model, SYBILL 2.3c interaction model, and the event selection described in Ref [71] for a three-neutrino model (salmon) and a 3+1 sterile neutrino model (black line) with $\sin^2(2\theta_{24}) = 0.1$, $\sin^2(2\theta_{34}) = 0.2$, and $\Delta m_{41}^2 = 4.5 \text{ eV}^2$. Number of events is summed over zenith angles (top) and energy (bottom) bins. Note that the oscillation signature is a correlated function of both variables, so appears very indistinctly in these projections.

calculated according to published reconstruction resolutions [3, 8]. Angular error in reconstruction is nominalized with a Kent Distribution [65] over azimuths to extract the zenith error. The width of the Kent distribution, θ_z^{err} , is energy-dependent according to the 50% angular error presented in Ref [8], so we solve for the parameter κ using

$$-\int_1^{\cos \theta_z^{err}(E_\nu^{true})} \frac{\kappa}{2 \sinh \kappa} e^{\kappa \cos \theta} d \cos \theta = 0.50 \quad (4)$$

at each analysis bin.

The expected number of events for ten years of livetime is shown on the bottom of Figure 3, and one-dimensional histograms of the number of events are shown in Figure 4.

B. Track Rates

In order to calculate the expected track event rate in IceCube, we use a Monte Carlo set published as part of a previous 1-year search for sterile neutrinos [6]. We use the same energy and cosine-zenith binning used in Subsection III A, and similarly scale the data to ten years of livetime. The expected number of tracks for ten years of livetime is shown in Figure 3, top panel.

IV. SYSTEMATIC UNCERTAINTIES

A detailed treatment of IceCube’s sources of systematic uncertainties would be prohibitively complex and require proprietary IceCube tools, so a truly rigorous sensitivity calculation for each channel can only be provided by the IceCube collaboration. Nevertheless, to estimate the expected impact of such effects we use publicly available data from Ref. [13] to apply a simplified treatment of the expected scale of systematic uncertainties. Dominant sources of systematic uncertainty are expected to derive from the shape and normalization of the atmospheric and astrophysical neutrino fluxes and the properties of the South Pole ice as in Ref. [13]. Other sources of uncertainty, such as the efficiencies of IceCube’s DOMs, neutrino and anti-neutrino interaction cross sections, were not used in this preliminary analysis since they are sub-leading effects.

Absorption and scattering of light in the ice are treated using the effective gradient approach developed in Ref. [2] and used by Ref. [12]. Uncertainties in the depth-dependence of the absorption and scattering of South Pole ice leads to uncertainties in energy reconstruction, and therefore an uncertainty in the energy-spectrum of expected event rates.

The one-sigma deviations to the cosmic-ray flux are considered as in Ref [13]. These deviations calculate the expected one-sigma shifts in the expected atmospheric neutrino rates. Similarly, we perturb the slope of the astrophysical neutrino flux to determine variances in expected astrophysical neutrino rates. Per-bin uncertainties are then summed in quadrature to calculate a net systematic uncertainty.

Overall normalization of fluxes is treated as a nuisance parameter and allowed to float freely, such that we are studying energy and zenith shape and flavor ratio effects only, and not the absolute neutrino rate. We fit to the normalization before calculating the log likelihood at each physics point. As will be described below, this simplified prescription has been tested by regenerating IceCube’s sensitivity to θ_{24} via ν_μ disappearance, and a similar median sensitivity to the published IceCube analysis is obtained (shown in Figure 5). Although both imperfect and incomplete, we believe that this prescription captures the majority of the important effects of the relevant systematic uncertainties for present purposes.

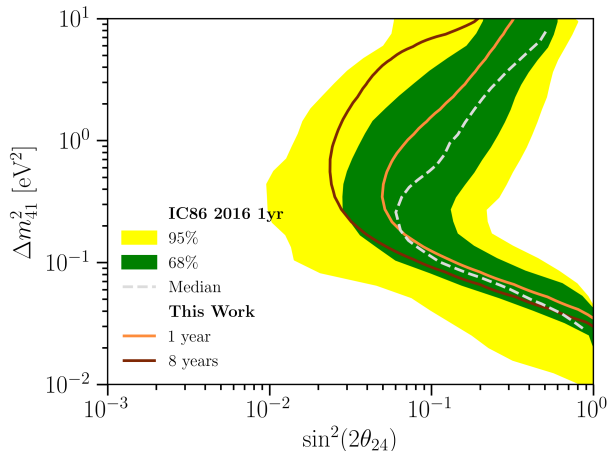


FIG. 5. 2 DOF, 90% C.L. sensitivity to $|U_{24}|^2$ and Δm_{41}^2 with $\theta_{34} = 0.0$. These results closely reproduce those of Ref. [13].

V. PREDICTED SENSITIVITIES

A binned-likelihood approach is used in calculating the log-likelihood for the expected numbers of events for each set of physical parameters. The test statistic at each point in parameter space is calculated according to,

$$\text{TS} = -2\Delta\text{LLH} = -2(\ln L - \ln L_{max}), \quad (5)$$

after removing the overall normalization effect by fitting the no-sterile-neutrinos flux to the parameter point of interest and adjusting the hypothesis normalization accordingly. We have performed likelihood based analyses in three samples, tracks only, cascades only, and tracks and cascades combined.

A. Tracks-only sensitivity to ν_μ disappearance

We first perform likelihood analysis for IceCube's track sample: calculating the sensitivity to θ_{24} and Δm_{41}^2 , using the procedure described in Section III to predict the expected number of tracks in only eight years of livetime. These results are shown in Figure 5, which accurately reproduce the sensitivities presented in Ref. [6]. We have chosen this point of comparison rather than the more recent results of Ref. [12] as the updated event selection there improves efficiencies at low energy, while the data release required to make these studies is only available at present for the earlier, one-year analysis. Approximate agreement of the median sensitivity, well within the bounds of expected fluctuations, validates our simplified analysis methodology as capturing the essential elements needed for a robust sensitivity estimate. For completeness we also present an eight-year projection.

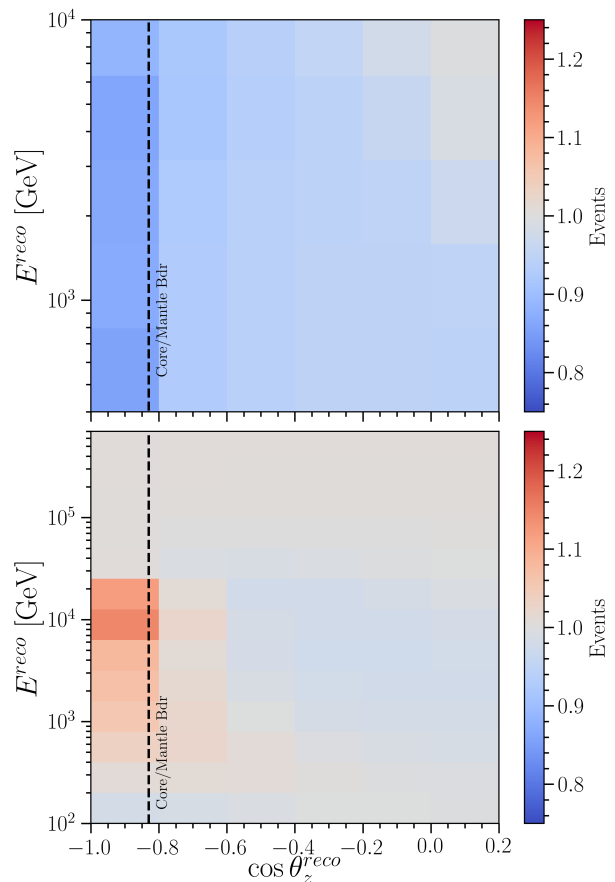


FIG. 6. Ratio of expected tracks (top) and cascades (bottom) for a sterile neutrino model with $\sin^2(2\theta_{24}) = 0.1$, $\sin^2(2\theta_{34}) = 0.2$, and $\Delta m_{41}^2 = 4.5 \text{ eV}^2$ and the standard three-neutrino model. Fluxes are calculated using the Hillas-Gaisser H3a cosmic ray flux model and the SYBILL 2.3c interaction model. A broad disappearance is expected in up-going tracks coincident with an appearance of up-going cascades.

B. Cascades-only sensitivity to ν_τ appearance

Signatures of ν_τ appearance require nonzero values for all of Δm_{41}^2 , θ_{24} , and θ_{34} . An example of a point with a non-trivial appearance signature that is consistent with existing experimental limits is shown in Figure 6. This signature in reconstructed space is calculated by fixing θ_{24} and Δm_{41}^2 at their best-fit points from IceCube's ν_μ disappearance searches, and fixing $\sin^2(2\theta_{34}) = 0.2$, comfortably consistent with current bounds, which are around $\sin^2(2\theta_{34}) \lesssim 0.6$ [9, 25].

Since all three of the above parameters must be nonzero to observe ν_τ appearance, sensitivities should be expressed in three dimensional spaces (or four, if θ_{14} is also included). However, to facilitate presentation of results on 2D plots in this work we have primarily opted to present two dimensional sensitivities under specific and experimentally motivated assumptions on the third parameter.

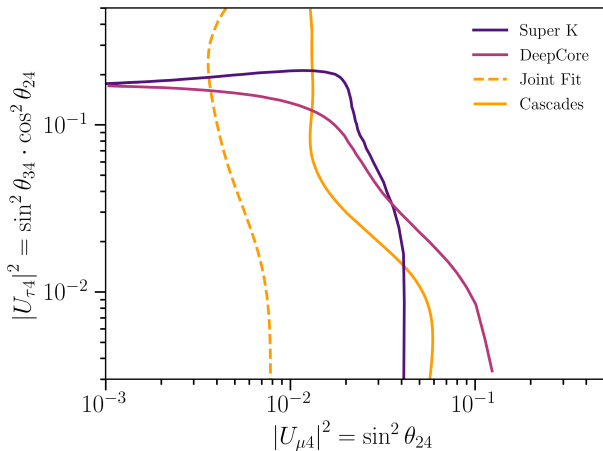


FIG. 7. The 2 DOF, 90% C.L. sensitivity to the θ_{24} and θ_{34} neutrino mixing parameters from this work with $\Delta m_{41}^2 = 1$ eV² for this work, IceCube’s DeepCore [9], and Super-Kamiokande [21]. The sensitivity through cascades is shown in the solid contour, and the joint track-cascade contour is dashed.

Using the methods described in Section III, we calculate expected cascade rates in IceCube at combinations of θ_{24} , θ_{34} , and Δm_{41}^2 . The effects of θ_{14} are marginal unless large mixing angles are reached, and so for this part of the analysis it was kept to zero. The matter effects on these oscillations are similarly only marginally affected by the CP-violating phases [13], and so they are fixed to zero. The results of the sensitivity scan over cascade events only are shown in the solid line of Figure 7, with sensitivities from other experiments overlaid, at the conventional benchmark point of $\Delta m_{41}^2 = 1$ eV²; sensitivities at other values of Δm_{41}^2 are shown in the solid lines of Figure 8. We see that with cascades alone we expect a sensitivity competitive with other leading sensitivities from Super-Kamiokande [21] and IceCube’s DeepCore [9]. Sensitivities are the most competitive for points in phase space where both θ_{24} and θ_{34} are large; here, the transition probability $P(\nu_\mu \rightarrow \nu_\tau)$ is maximized.

Meanwhile, in regions where $|U_{\tau 4}|^2$ is small, ν_μ disappearance is most significant in a signal similar to Refs. [12, 13], but as ν_μ cascades. A small increase to $|U_{\tau 4}|^2$ can then lead to competing ν_τ appearance and ν_μ disappearance, and so for small values of Δm_{41}^2 , this leads to a reduction of sensitivity. Since ν_μ events overwhelmingly lead to cascades while ν_τ often cause tracks, at higher $|U_{\mu 4}|^2$ the ν_τ appearance begins to dominate and sensitivity improves. Finally, since tau appearance follows a $\nu_\mu \rightarrow \nu_s \rightarrow \nu_\tau$ appearance channel, a non-zero $|U_{\mu 4}|^2$ is needed to for any sensitivity; this causes a lower bound on the $|U_{\mu 4}|^2$ sensitivity.

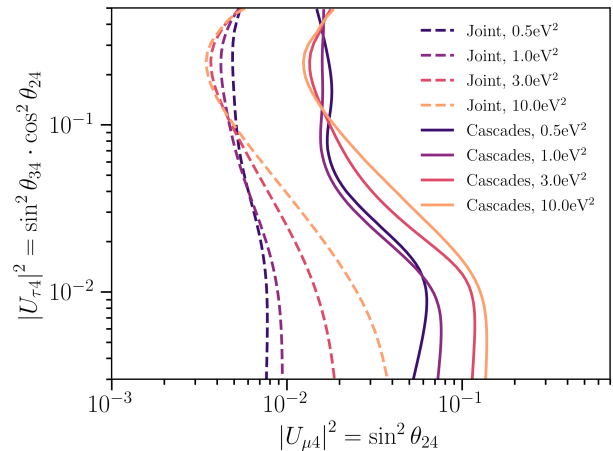


FIG. 8. Cross-sections of the 3 DOF, 90% C.L. sensitivity surface to θ_{24} , θ_{34} , and Δm_{41}^2 . The sensitivity through cascades is shown in the solid contour, and the joint track-cascade contour is dashed.

C. Joint Sensitivity for ν_μ disappearance and ν_τ appearance

By performing a joint sensitivity using both cascade and track-like events, we are able to significantly improve the sensitivity, by exploring a flavor ratio rather than a pure shape effect. Track-like events will provide a method to fit to the overall flux normalization and further constrain sensitivities. Specifically, the process described in in Subsection VB is performed for track events, and the fit event-number normalization is then used in calculating the log likelihood in the cascade channel. The combined likelihood for both is then used in determining sensitivity contours. These results are shown in Figure 7. A significant sensitivity enhancement relative to either tracks or cascades alone is obtained.

In addition to calculating sensitivity, we examine the results that may be expected in the presence of a sterile neutrino with non-zero θ_{24} and θ_{34} . In Figure 9 we show the result obtained by injecting a signal with $\sin^2(2\theta_{24}) = 0.1$, $\sin^2(2\theta_{34}) = 0.2$ and $\Delta m_{41}^2 = 4.64$ eV² and fitting over values of the mixing parameters; this mass squared splitting was chosen out of computational convenience as it lines up with a point at which fluxes were calculated. We include four slices through the space in Δm_{41}^2 at several benchmark points, and provide contours at 90% CL calculated using χ^2 assuming that the test statistic, TS, satisfies Wilk’s theorem and is distributed with a χ^2 distribution with thresholds with thresholds consistent with three degrees of freedom. A signature of this form, which is consistent with present constraints would be potentially discoverable in a joint tracks and cascades analysis at IceCube.

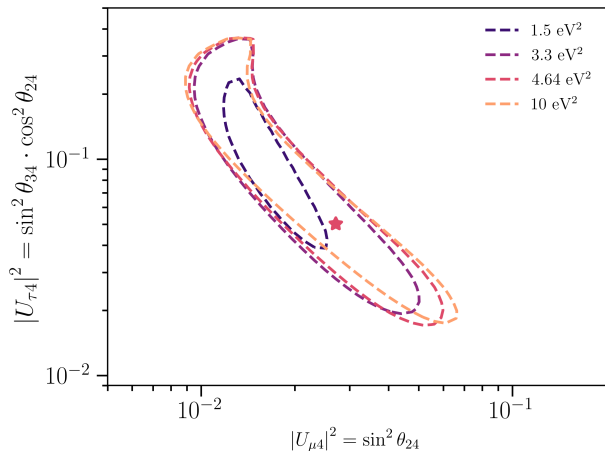


FIG. 9. 3 DOF, 90% C.L. sensitivity to the $|U_{\mu 4}|^2$ and $|U_{\tau 4}|^2$ PMNS matrix elements, at various values of Δm_{41}^2 , for this work using a joint track-cascade likelihood assuming a sterile neutrino with $\sin^2(2\theta_{24}) = 0.1$, $\sin^2(2\theta_{34}) = 0.2$, and $\Delta m_{41}^2 = 4.64 \text{ eV}^2$.

D. Joint Sensitivity for ν_μ and disappearance generic cascade appearance

Cascade appearance may be introduced not only from ν_τ appearance, but also from ν_e appearance. A non-zero value for θ_{14} is motivated in particular by recent results from the BEST experiment, which motivates us to consider whether IceCube fitting both cascade and track channels has sensitivity to values of θ_{14} consistent with such a ν_e disappearance effect. IceCube can of course not rule out the BEST anomaly alone, since a scenario with $\theta_{24} = 0$ will generate no substantial appearance signatures in IceCube for any value of θ_{14} . But in principle it may be able confirm the BEST anomaly, given sizeable enough values for both θ_{24} and θ_{14} . In such a model with non-zero θ_{14} , θ_{24} , and θ_{34} , resonant oscillations lead to appearances in both the ν_τ and ν_e channels shown in Figure 10, wherein the BEST best-fit values were used for θ_{14} and Δm_{41}^2 .

To assess sensitivity to this effect in IceCube, scans over θ_{14} and θ_{34} were performed at multiple values of Δm_{41}^2 and θ_{24} . In Figure 11 we show IceCube's sensitivity to a 3+1 sterile neutrino model with $\theta_{14} = 0.0$. These contours represent the median expected 90% confidence level that could be drawn if no sterile neutrino were present, given assumptions on the non-plotted parameters shown in the caption. The two choices of assumptions made on the non-fitted parameters correspond to $\theta_{24} = 0.1609$ (the ν_μ disappearance best fit point from Ref. [12]) or $\theta_{24} = 0.3826$ (a value within the 90% results contour of Ref. [12]), and $\Delta m_{41}^2 = 1 \text{ eV}^2$ (a standard benchmark point in the field), $\Delta m_{41}^2 = 3.3 \text{ eV}^2$ (the BEST best-fit point), and $\Delta m_{41}^2 = 4.64 \text{ eV}^2$ (close to the IceCube ν_μ disappearance best fit point at 4.5 eV^2). It is

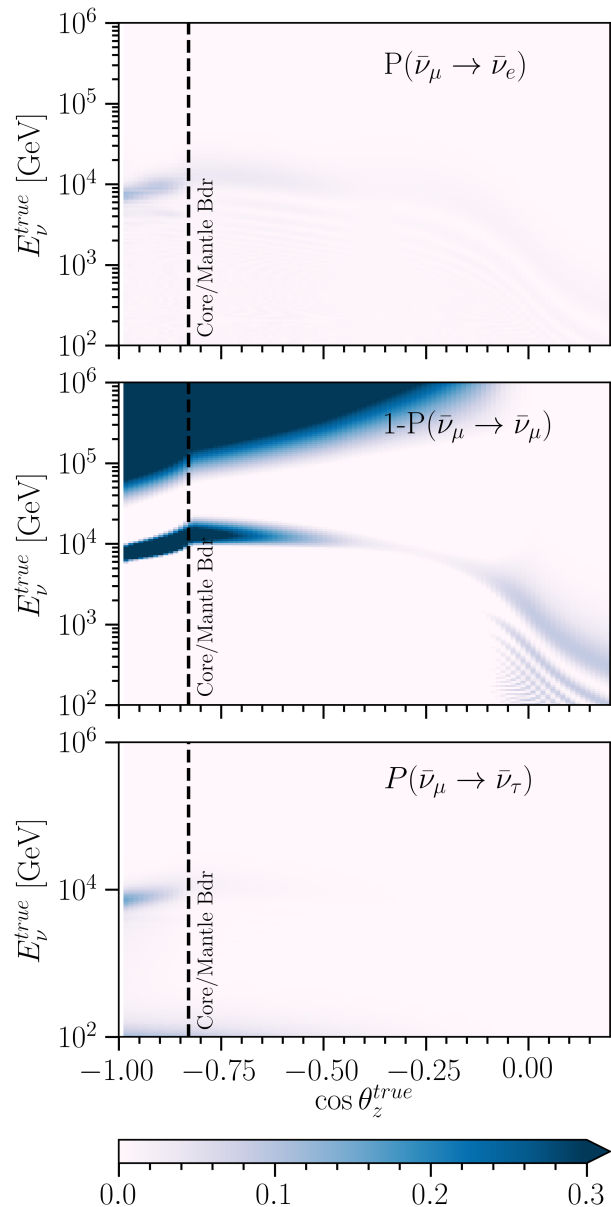


FIG. 10. Transition probabilities $P(\bar{\nu}_\mu \rightarrow \bar{\nu}_\alpha)$ for $\bar{\nu}_e$ (top), $\bar{\nu}_\mu$ (middle), and $\bar{\nu}_\tau$ (bottom) for a sterile neutrino flux with $\sin^2(2\theta_{14}) = 0.43$, $\sin^2(2\theta_{24}) = 0.1$, $\sin^2(2\theta_{34}) = 0.01$, and $\Delta m_{41}^2 = 3.3 \text{ eV}^2$. A dashed black line is used to denote the outer core-mantle boundary.

observed that IceCube has significant sensitivity in this high dimensional parameter space for many values of the mixing parameters consistent with the present BEST and IceCube results, assuming a non-zero value of θ_{24} consistent with IceCube's existing preferred regions from ν_μ disappearance measurements.

A more intuitive picture of IceCube's capability to confirm the BEST anomaly as being sterile-neutrino related, given values of other mixing parameters consistent with IceCube and world data, is shown in Fig. 12. Here, like-

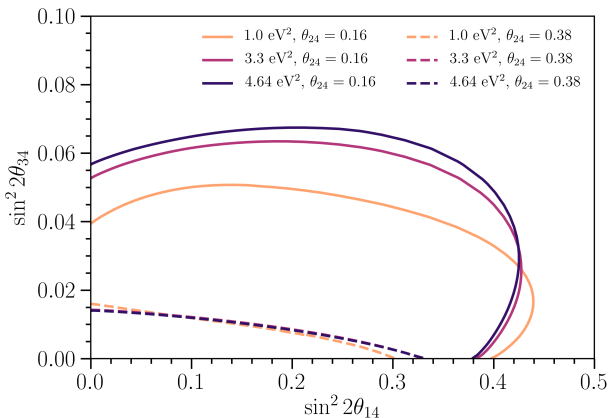


FIG. 11. The 2 DOF, 90% C.L. sensitivity contours for $\sin^2 \theta_{14}$ and $\sin^2 \theta_{34}$, using a joint track-cascade likelihood, for a 3+1 sterile neutrino model with various values of Δm_{41}^2 and θ_{24} , and $\theta_{14} = 0.0$.

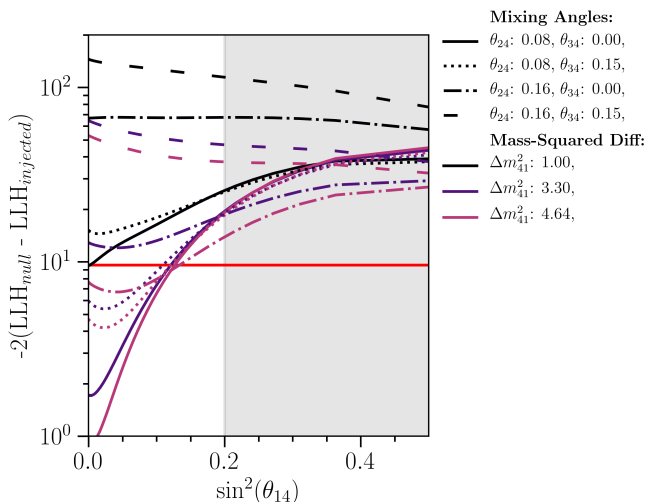


FIG. 12. The test statistics values for various different injected 3+1 sterile neutrino models, using a joint track-cascade likelihood, compared to a three-neutrino hypothesis. The red line represents a 4 DOF 95% CL sensitivity threshold; the shaded region represents the 95% confidence level bounds from the BEST best fit.

likelihoods are calculated according to injected sterile neutrino parameters and assuming a three-neutrino model; the resulting test statistics are shown. For all considered combinations, IceCube is seen to be capable of discriminating a BEST-like sterile neutrino flux from a three-neutrino model at the 95% confidence level. Thus, IceCube appears to have capability to confirm the best anomaly at least 95% confidence, given suitable values of the other mixing parameters, within existing constraints

and uncertainties.

VI. CONCLUSIONS

We have considered IceCube's sensitivity to sterile neutrinos through the cascade appearance channel. Both ν_τ and ν_e appearance signatures are in principle observable by IceCube for θ_{14} and θ_{34} values within existing constraints, θ_{24} around IceCube's present preferred values from ν_μ disappearance, and many possible values Δm_{41}^2 .

We find that IceCube's sensitivity in the joint $U_{\tau 4}$, $U_{\mu 4}$ space that has been explored by previous analyses at SuperKamiokande and IceCube will be enhanced significantly at the benchmark point of $\Delta m^2 = 1 \text{ eV}^2$ by a joint fit to both track and cascade samples. Strong sensitivity is also obtained for other mass points, under the standard mixing assumption of $\theta_{14} = 0$. Cascade signatures that may accompany tentative but weak hints of ν_μ disappearance for $\Delta m_{41}^2 \sim 4.5 \text{ eV}^2$ and $\sin^2(\theta_{24}) \sim 0.1$ are discoverable at IceCube with values θ_{34} that remain consistent with world data, strongly motivating investigation of ν_τ appearance via cascades in parallel with the established IceCube searches for ν_μ disappearance using tracks.

We have also explored the effect of introducing non-trivial ν_e appearance, consistent with the BEST and gallium anomalies, via non-zero θ_{14} . IceCube cannot rule out the BEST or gallium preferred regions in θ_{14} alone, since sensitivity of IceCube to this parameter requires non-zero θ_{24} . For modest values of θ_{24} at either the IceCube best fit point in ν_μ disappearance or at a point near the 90% CL upper limit in this channel, however, values of θ_{14} and Δm_{41}^2 around the best fit point can be probed at better than 90% confidence level.

We conclude that our joint analysis of track and cascade topologies at IceCube can contribute to the ongoing worldwide project of understanding short baseline anomalies in both ν_e appearance and disappearance channels. The IceCube data set, probing both ν_μ disappearance and ν_e and ν_τ appearance near the matter resonance for core crossing neutrinos, provides unique and powerful insights into possible mixing of heavier neutrino mass states with the ν_τ flavor, as well as offering sensitivity to ν_e appearance in experimentally relevant parts of parameter space associated with the BEST and gallium anomalies.

VII. ACKNOWLEDGMENTS

BS and BJPJ are supported by the National Science Foundation under award number 1913607. CAA is supported by the Faculty of Arts and Sciences of Harvard University, and the Alfred P. Sloan Foundation. JC and AD are supported by the National Science Foundation under award number 1912764.

-
- [1] Aartsen, M. *et al.* (IceCube), *Journal of Instrumentation* **12**, P03012 (2017).
- [2] Aartsen, M. *et al.* (IceCube), *Journal of Cosmology and Astroparticle Physics* **2019**, 048–048 (2019).
- [3] Aartsen, M. G. *et al.* (IceCube), *Journal of Instrumentation* **9**, P03009–P03009 (2014).
- [4] Aartsen, M. G. *et al.* (IceCube), *Phys. Rev. D* **91**, 022001 (2015).
- [5] Aartsen, M. G. *et al.* (IceCube), *Physical Review Letters* **114** (2015), 10.1103/physrevlett.114.171102.
- [6] Aartsen, M. G. *et al.* (IceCube), *Phys. Rev. Lett.* **117**, 071801 (2016).
- [7] Aartsen, M. G. *et al.* (IceCube), *The Astrophysical Journal* **835**, 151 (2017).
- [8] Aartsen, M. G. *et al.* (IceCube), *The Astrophysical Journal* **846**, 136 (2017).
- [9] Aartsen, M. G. *et al.* (IceCube), *Physical Review D* **95** (2017), 10.1103/physrevd.95.112002.
- [10] Aartsen, M. G. *et al.* (IceCube), *Physical Review D* **99** (2019), 10.1103/physrevd.99.032004.
- [11] Aartsen, M. G. *et al.* (IceCube), *Physical Review Letters* **125** (2020), 10.1103/physrevlett.125.121104.
- [12] Aartsen, M. G. *et al.* (IceCube), *Physical Review Letters* **125** (2020), 10.1103/physrevlett.125.141801.
- [13] Aartsen, M. G. *et al.* (IceCube), *Physical Review D* **102** (2020), 10.1103/physrevd.102.052009.
- [14] Aartsen, M. G. *et al.* (IceCube), *Nature* **591**, 220 (2021), [Erratum: *Nature* 592, E11 (2021)].
- [15] Abazajian, K. N. *et al.*, “Light Sterile Neutrinos: A White Paper,” (2012), arXiv:1204.5379 [hep-ph].
- [16] Abbasi, R. *et al.* (IceCube), *Nuclear Instruments and Methods in Physics Research Section A: Accelerators, Spectrometers, Detectors and Associated Equipment* **601**, 294 (2009).
- [17] Abbasi, R. *et al.* (IceCube), *Astroparticle Physics* **35**, 615 (2012).
- [18] Abbasi, R. *et al.* (IceCube), “Measurement of Astrophysical Tau Neutrinos in IceCube’s High-Energy Starting Events,” (2020), arXiv:2011.03561 [hep-ex].
- [19] Abbasi, R. *et al.* (IceCube), *Physical Review D* **104** (2021), 10.1103/physrevd.104.022002.
- [20] Abdurashitov, J. N. *et al.*, *Phys. Rev. C* **73**, 045805 (2006).
- [21] Abe, K. *et al.* (Super-Kamiokande Collaboration), *Phys. Rev. D* **91**, 052019 (2015).
- [22] Abratenko, P. *et al.* (MicroBooNE), “Search for an anomalous excess of charged-current ν_e interactions without pions in the final state with the MicroBooNE experiment,” (2021), arXiv:2110.14065 [hep-ex].
- [23] Abratenko, P. *et al.*, “Search for an anomalous excess of charged-current quasi-elastic ν_e interactions with the microboone experiment using deep-learning-based reconstruction,” (2021), arXiv:2110.14080 [hep-ex].
- [24] Abratenko, P. *et al.*, “Search for an excess of electron neutrino interactions in microboone using multiple final state topologies,” (2021), arXiv:2110.14054 [hep-ex].
- [25] Adamson, P. *et al.*, *Physical Review Letters* **107** (2011), 10.1103/physrevlett.107.011802.
- [26] Aguilar-Arevalo, A. *et al.*, *Physical Review Letters* **121** (2018), 10.1103/physrevlett.121.221801.
- [27] Aguilar-Arevalo, A. A. and Bothers, (MiniBooNE Collaboration), *Phys. Rev. Lett.* **121**, 221801 (2018).
- [28] Akhmedov, E. K., *Sov. J. Nucl. Phys.* **47**, 301 (1988).
- [29] Akhmedov, E. K. and Smirnov, A. Y., *Physical Review Letters* **85**, 3978–3978 (2000).
- [30] Argüelles, C. A., Farrag, K., Katori, T., Khandelwal, R., Mandalia, S., and Salvado, J., *Journal of Cosmology and Astroparticle Physics* **2020**, 015–015 (2020).
- [31] Argüelles, C. A., Salvado, J., and Weaver, C. N., (2014), arXiv:1412.3832 [hep-ph].
- [32] Argüelles, C. A., Salvado, J., and Weaver, C. N., “nuSQuIDS,” <https://github.com/Arguelles/nuSQuIDS>, (2015).
- [33] Argüelles, C. A. *et al.*, “MicroBooNE and the ν_e Interpretation of the MiniBooNE Low-Energy Excess,” (2021), arXiv:2111.10359 [hep-ph].
- [34] Athanassopoulos, C. *et al.* (LSND), *Physical Review Letters* **81**, 1774–1777 (1998).
- [35] Athar, H., Kim, C. S., and Lee, J., *Modern Physics Letters A* **21**, 1049–1065 (2006).
- [36] Barger, V., Gao, Y., and Marfatia, D., *Physical Review D* **85** (2012), 10.1103/physrevd.85.011302.
- [37] Barinov, V. V. *et al.* (BEST), “Results from the Baksan Experiment on Sterile Transitions (BEST),” (2021), arXiv:2109.11482 [nucl-ex].
- [38] Beacom, J. F., Bell, N. F., Hooper, D., Pakvasa, S., and Weiler, T. J., *Phys. Rev. D* **68**, 093005 (2003).
- [39] Berns, L. (T2K), in *55th Rencontres de Moriond on Electroweak Interactions and Unified Theories* (2021) arXiv:2105.06732 [hep-ex].
- [40] Capozzi, F., Lisi, E., Marrone, A., Montanino, D., and Palazzo, A., *Nuclear Physics B* **908**, 218–234 (2016).
- [41] Carlos A. Argüelles and Jordi Salvado and Christopher N. Weaver, “nusquids: A toolbox for neutrino propagation,” (2021), arXiv:2112.13804 [hep-ph].
- [42] Chizhov, M., Maris, M., and Petcov, S. T., (1998), arXiv:hep-ph/9810501.
- [43] Chizhov, M. V. and Petcov, S. T., *Physical Review Letters* **83**, 1096–1099 (1999).
- [44] Choubey, S., *Journal of High Energy Physics* **2007**, 014–014 (2007).
- [45] Cirelli, M., Marandella, G., Strumia, A., and Vissani, F., *Nuclear Physics B* **708**, 215–267 (2005).
- [46] Cooper-Sarkar, A., Mertsch, P., and Sarkar, S., *JHEP* **08**, 042 (2011), arXiv:1106.3723 [hep-ph].
- [47] Dentler, M., Hernández-Cabezudo, Á., Kopp, J., Maltoni, M., and Schwetz, T., *Journal of High Energy Physics* **2017** (2017), 10.1007/jhep11(2017)099.
- [48] Denton, P. B., “Sterile Neutrino Searches with MicroBooNE: Electron Neutrino Disappearance,” (2021), arXiv:2111.05793 [hep-ph].
- [49] Diaz, A., Argüelles, C., Collin, G., Conrad, J., and Shaevitz, M., *Physics Reports* **884**, 1–59 (2020).
- [50] Dziewonski, A. M. and Anderson, D. L., *Physics of the Earth and Planetary Interiors* **25**, 297 (1981).
- [51] Esmaili, A., Halzen, F., and Peres, O., *Journal of Cosmology and Astroparticle Physics* **2012**, 041–041 (2012).
- [52] Esmaili, A., Halzen, F., and Peres, O., *Journal of Cosmology and Astroparticle Physics* **2013**, 048–048 (2013).
- [53] Esmaili, A. and Smirnov, A., *Journal of High Energy Physics* **2013**, 1 (2013).

- [54] Esteban, I., Gonzalez-Garcia, M., Maltoni, M., Schwetz, T., and Zhou, A., *Journal of High Energy Physics* **2020** (2020), 10.1007/jhep09(2020)178.
- [55] Esteban, I., Gonzalez-Garcia, M. C., Hernandez-Cabezudo, A., Maltoni, M., and Schwetz, T., *Journal of High Energy Physics* **2019** (2019), 10.1007/jhep01(2019)106.
- [56] Fedynitch, A. *et al.*, “Calculation of conventional and prompt lepton fluxes at very high energy,” (2015), arXiv:1503.00544 [hep-ph].
- [57] Gaisser, T. K., *Astroparticle Physics* **35**, 801 (2012).
- [58] Gandhi, R., Quigg, C., Hall Reno, M., and Sarcevic, I., *Astroparticle Physics* **5**, 81–110 (1996).
- [59] Gariazzo, S., Giunti, C., Laveder, M., and Li, Y. F., *Journal of High Energy Physics* **2017** (2017), 10.1007/jhep06(2017)135.
- [60] Giunti, C. and Laveder, M., *Physical Review C* **83** (2011), 10.1103/physrevc.83.065504.
- [61] Glashow, S. L., *Phys. Rev.* **118**, 316 (1960).
- [62] Gonzalez-Garcia, M. C., Halzen, F., and Maltoni, M., *Physical Review D* **71** (2005), 10.1103/physrevd.71.093010.
- [63] Halzen, F. and Saltzberg, D., *Phys. Rev. Lett.* **81**, 4305 (1998).
- [64] Hörandel, J. R., *Astroparticle Physics* **19**, 193–220 (2003).
- [65] Kent, J. T., *Journal of the Royal Statistical Society. Series B (Methodological)* **44**, 71 (1982).
- [66] Kopp, J. *et al.*, *Journal of High Energy Physics* **2013**, 1 (2013).
- [67] Krastev, P. and Smirnov, A., *Physics Letters B* **226**, 341 (1989).
- [68] Lindner, M., Rodejohann, W., and Xu, X.-J., *Journal of High Energy Physics* **2016** (2016), 10.1007/jhep01(2016)124.
- [69] Machado, P. A. *et al.*, *Annual Review of Nuclear and Particle Science* **69**, 363–387 (2019).
- [70] Mention, G., Fechner, M., Lasserre, T., Mueller, T. A., Lhuillier, D., Cribier, M., and Letourneau, A., *Physical Review D* **83**, 073006 (2011).
- [71] Niederhausen, H., *Measurement of the High Energy Astrophysical Neutrino Flux Using Electron and Tau Neutrinos Observed in Four Years of IceCube Data*, Ph.D. thesis, State University of New York at Stony Brook (2018).
- [72] Nunokawa, H. *et al.*, *Physics Letters B* **562**, 279–290 (2003).
- [73] Ostapchenko, S., *Physical Review D* **83** (2011), 10.1103/physrevd.83.014018.
- [74] Petcov, S. T., *International Journal of Modern Physics A* **32**, 1750018 (2017).
- [75] Riehn, F. *et al.*, *PoS ICRC2017*, 301 (2018), arXiv:1709.07227 [hep-ph].
- [76] de Salas, P., Forero, D., Ternes, C., Tórtola, M., and Valle, J., *Physics Letters B* **782**, 633–640 (2018).
- [77] Schael, S. *et al.* (ALEPH, DELPHI, L3, OPAL, SLD, LEP Electroweak Working Group, SLD Electroweak Group, SLD Heavy Flavour Group), *Phys. Rept.* **427**, 257 (2006), arXiv:hep-ex/0509008.
- [78] Serebrov, A. P. *et al.*, *JETP Letters* **109**, 213 (2019).
- [79] Tanabashi, M. *et al.* (Particle Data Group), *Phys. Rev. D* **98**, 030001 (2018).
- [80] Wang, Y. and Yasuda, O., “Search for sterile neutrinos by shower events at a future neutrino telescope,” (2021), arXiv:2110.12655 [hep-ph].